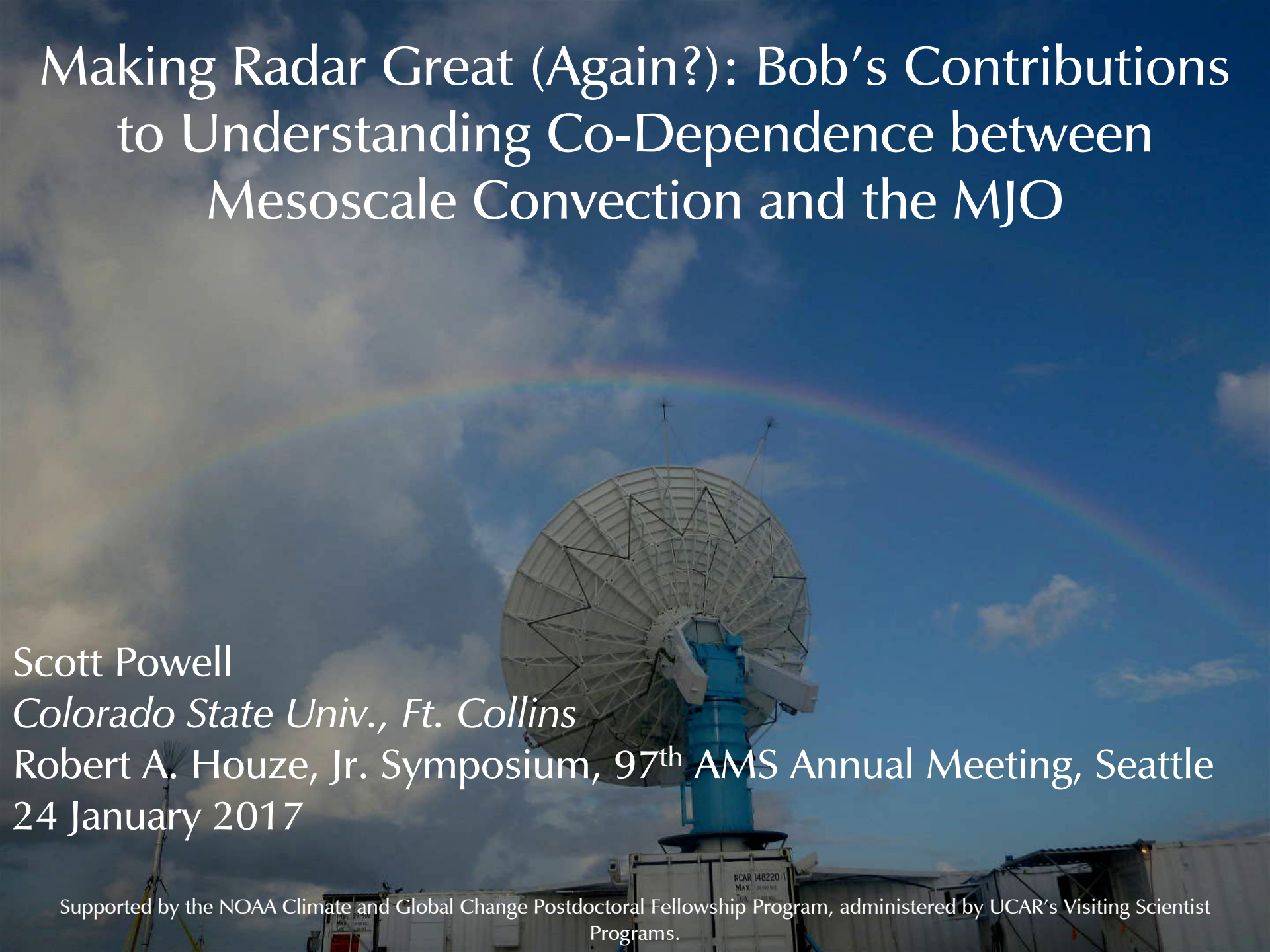


# Making Radar Great (Again?): Bob's Contributions to Understanding Co-Dependence between Mesoscale Convection and the MJO

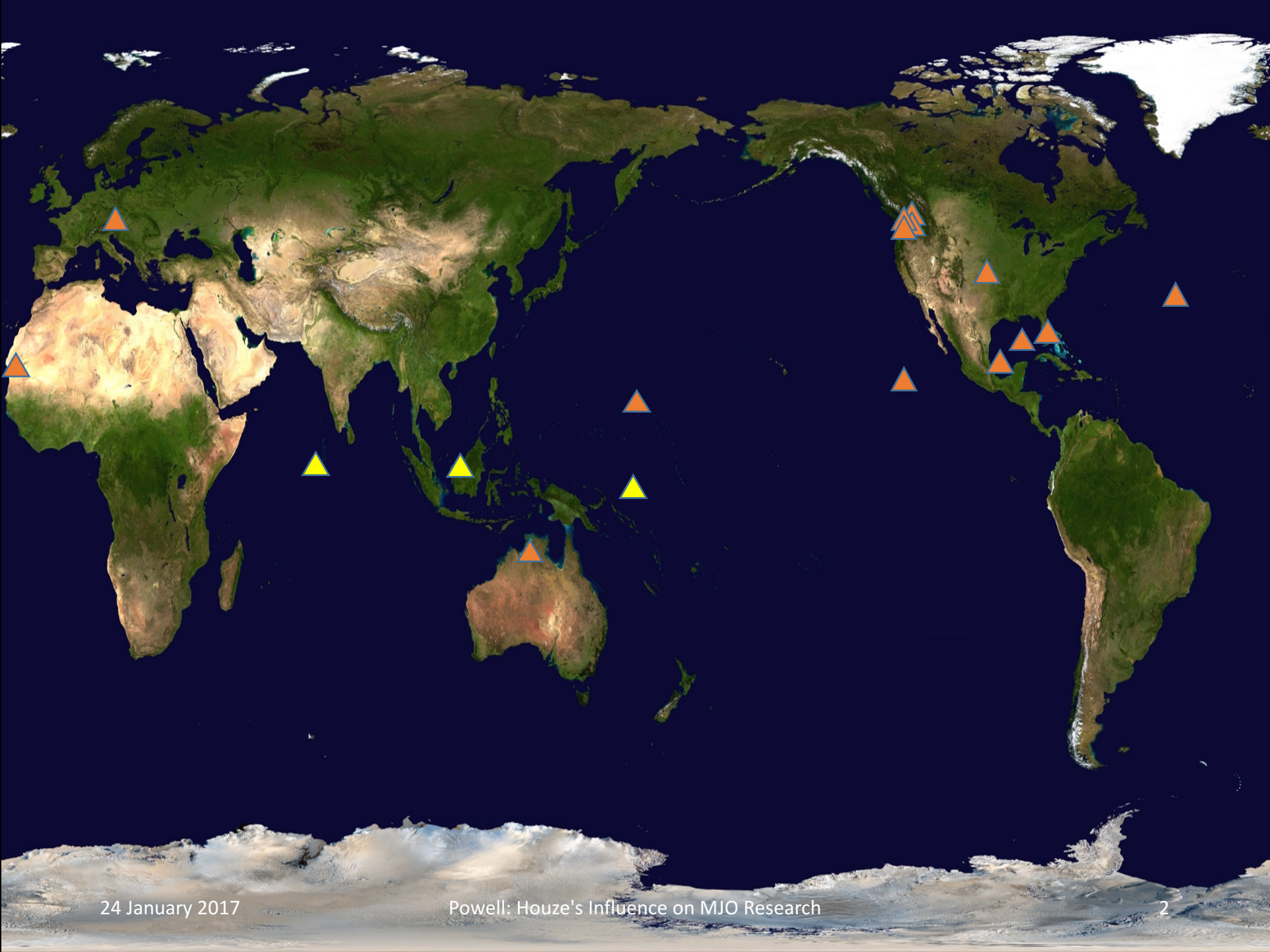


Scott Powell

*Colorado State Univ., Ft. Collins*

Robert A. Houze, Jr. Symposium, 97<sup>th</sup> AMS Annual Meeting, Seattle  
24 January 2017

Supported by the NOAA Climate and Global Change Postdoctoral Fellowship Program, administered by UCAR's Visiting Scientist Programs.





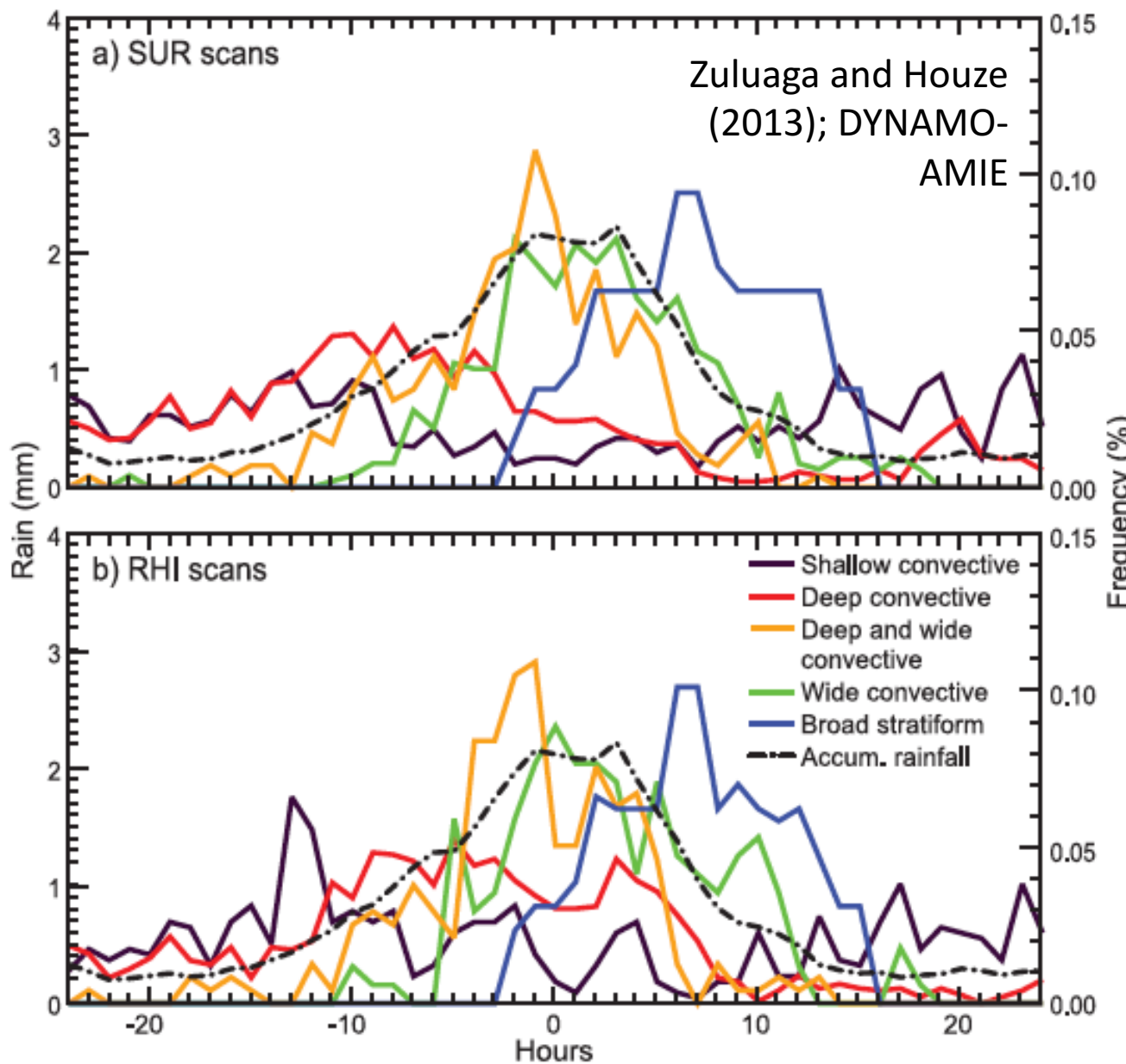
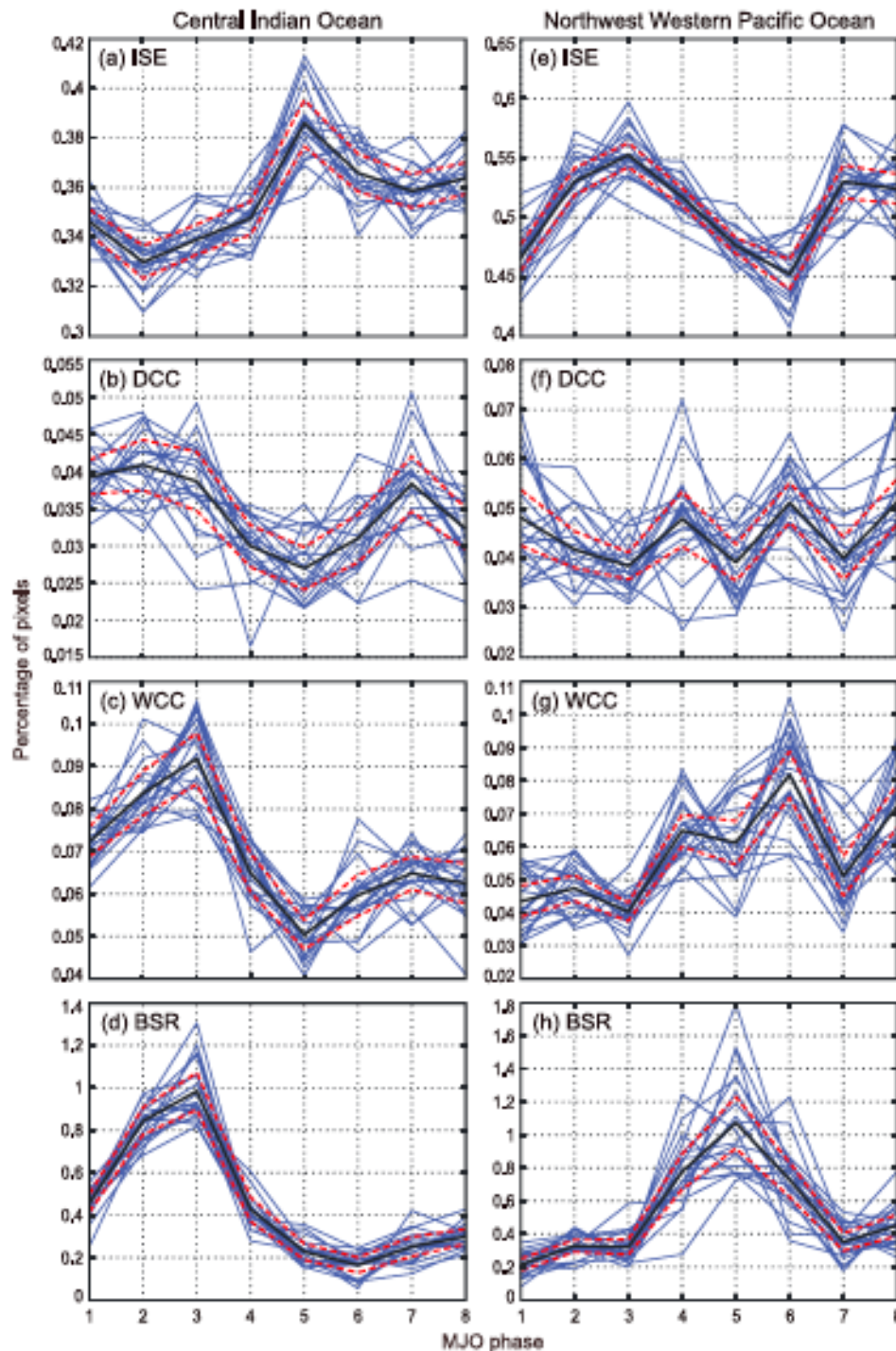
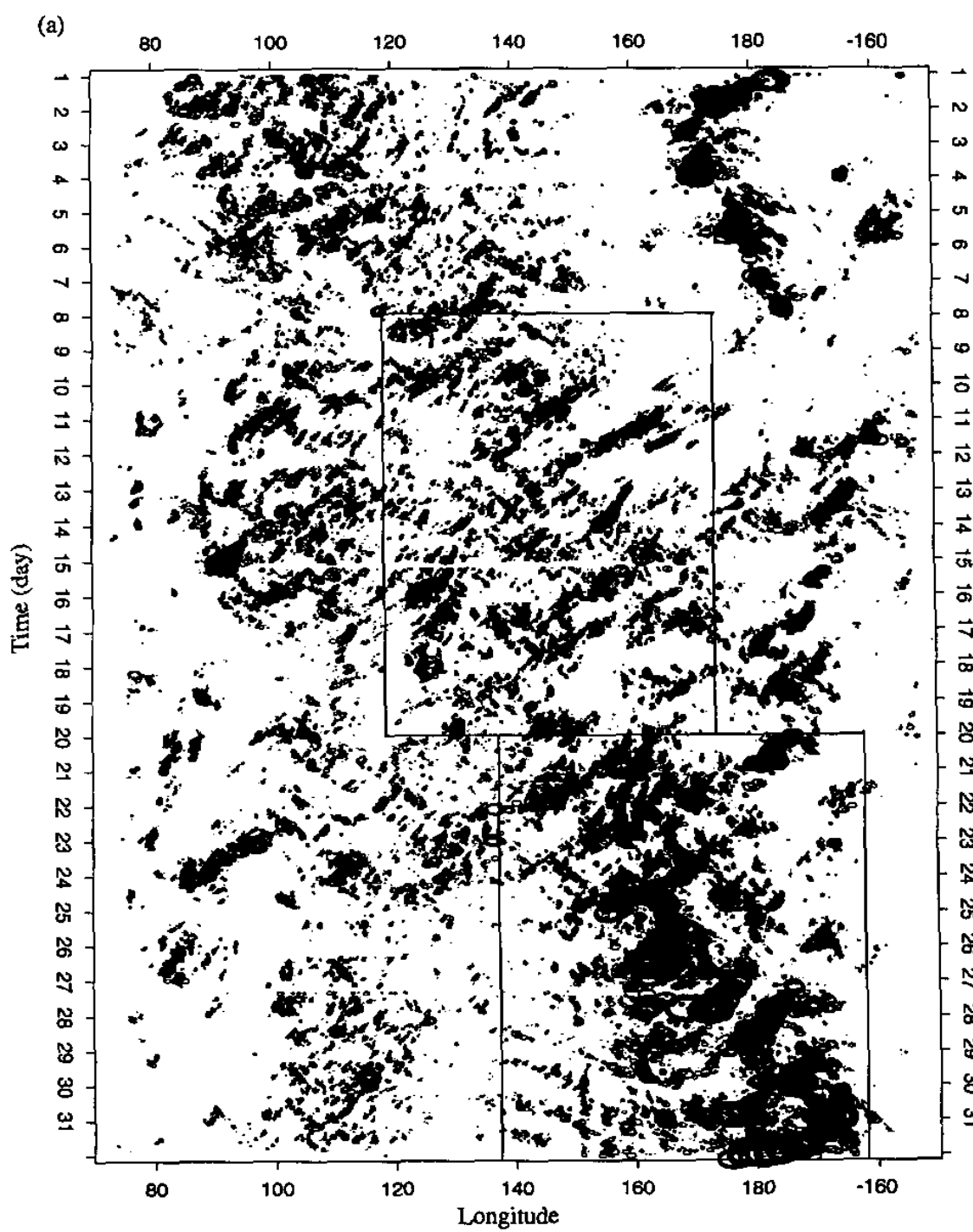


FIG. 3. Composites of the frequency of occurrence of each of the different types of radar echo structure defined in section 2 during 24 h before (negative time) and after (positive time) the composite maximum in rain accumulation (dash-dotted curve) calculated with (a) SUR and (b) RHI scanning strategy data. The right y axis is for the colored curves. The rainfall accumulation composite is computed by centering each of the 11 rain episodes in Fig. 2 on the time of the maximum of its running-mean curve in Fig. 2.



Chen et  
al. (1996)

TOGA  
COARE



Chen et  
al. (1996)

TOGA  
COARE

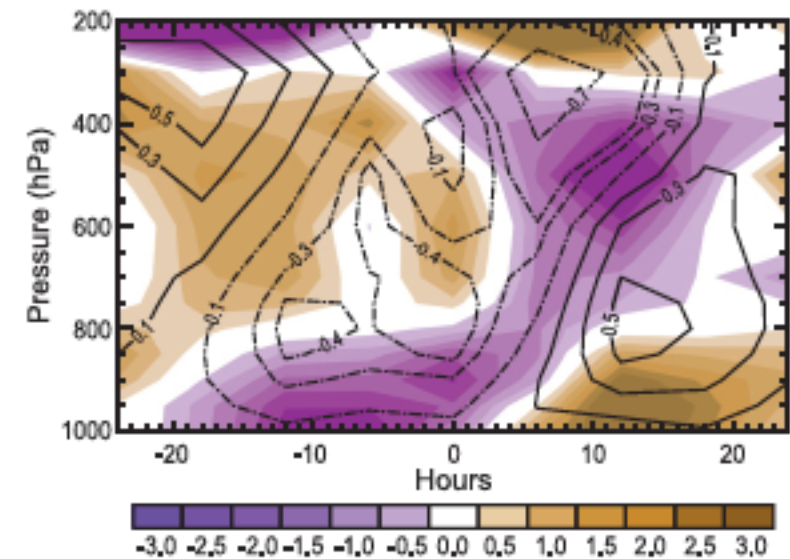
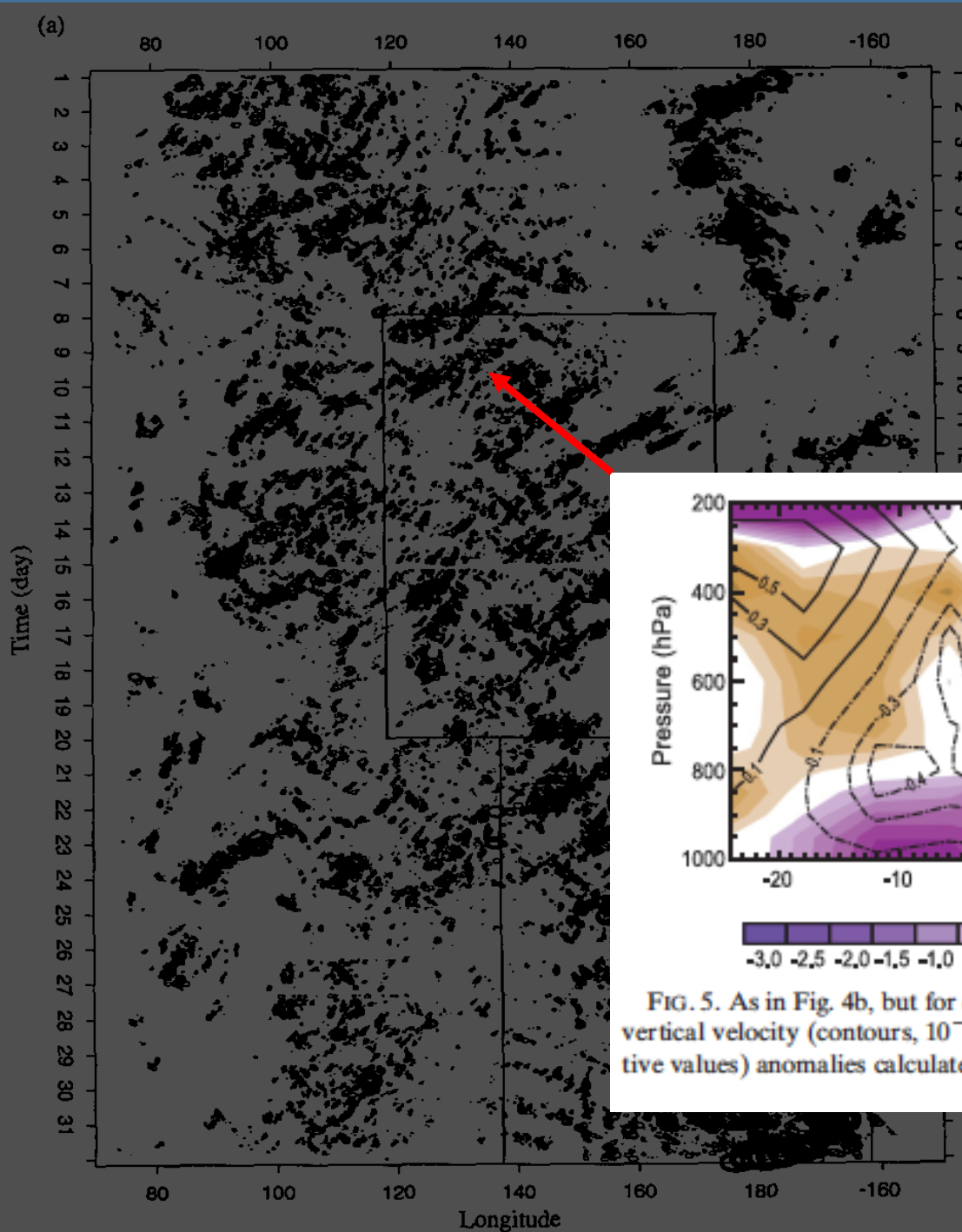
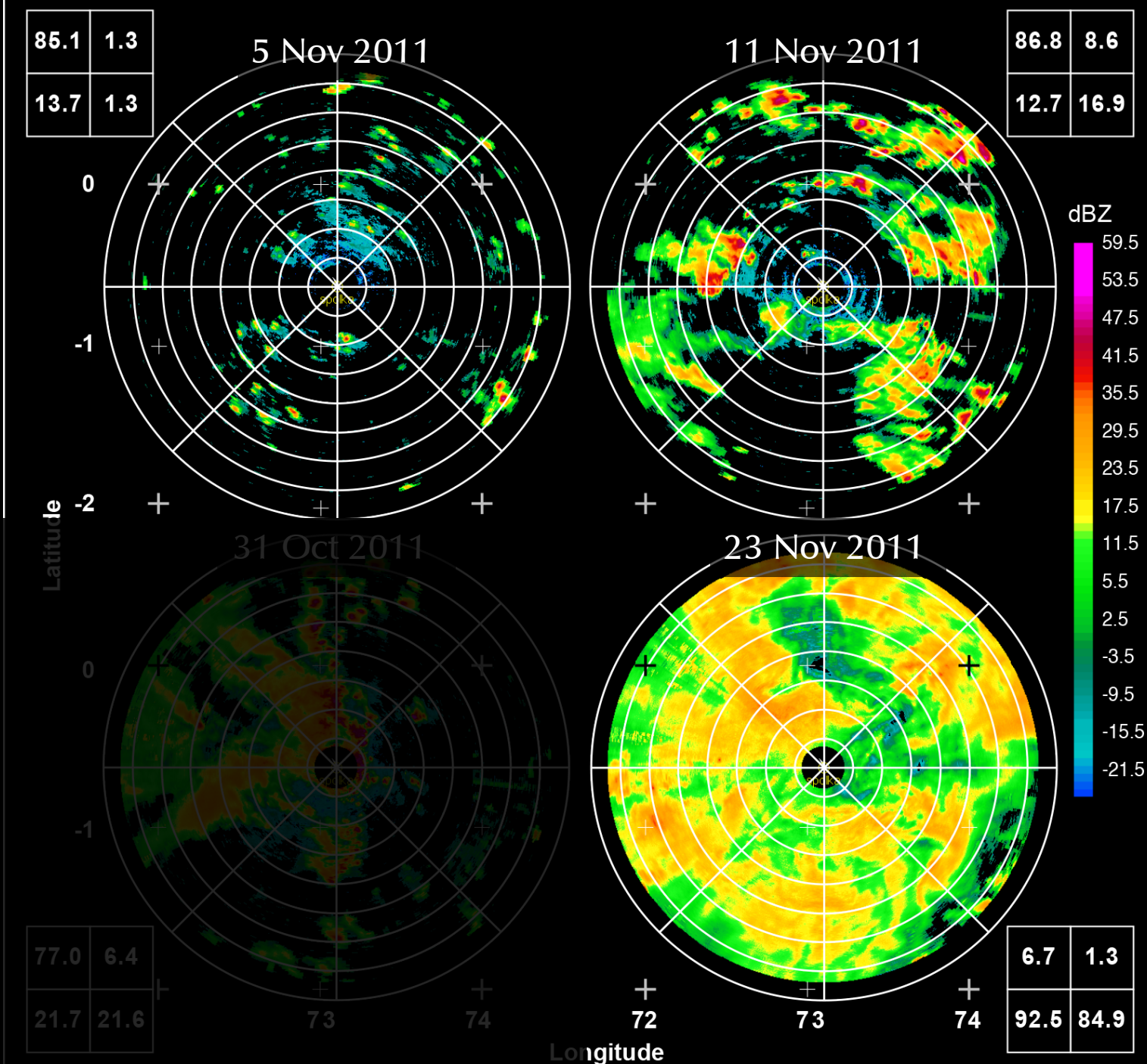
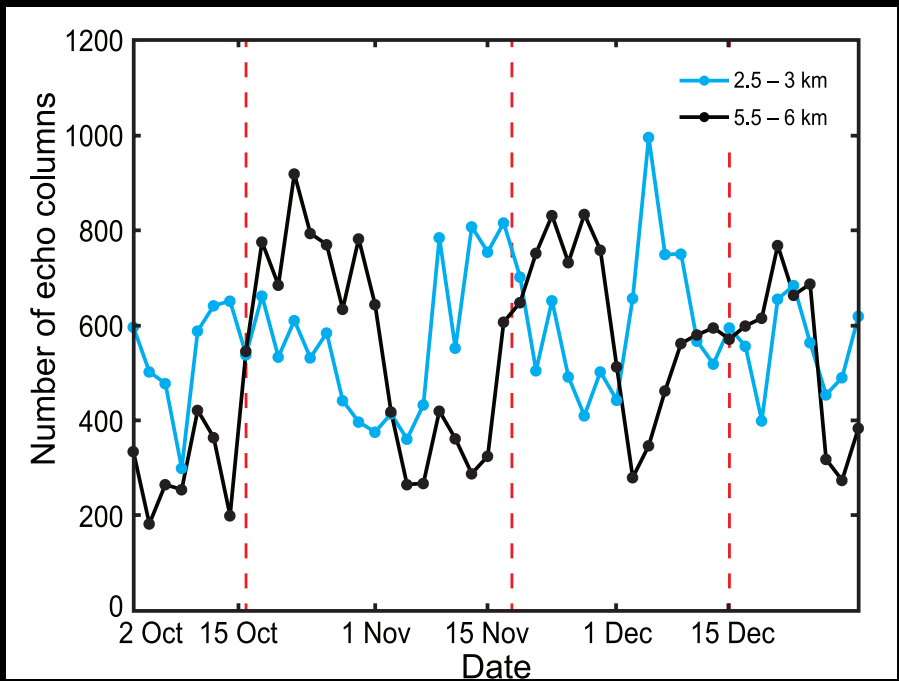
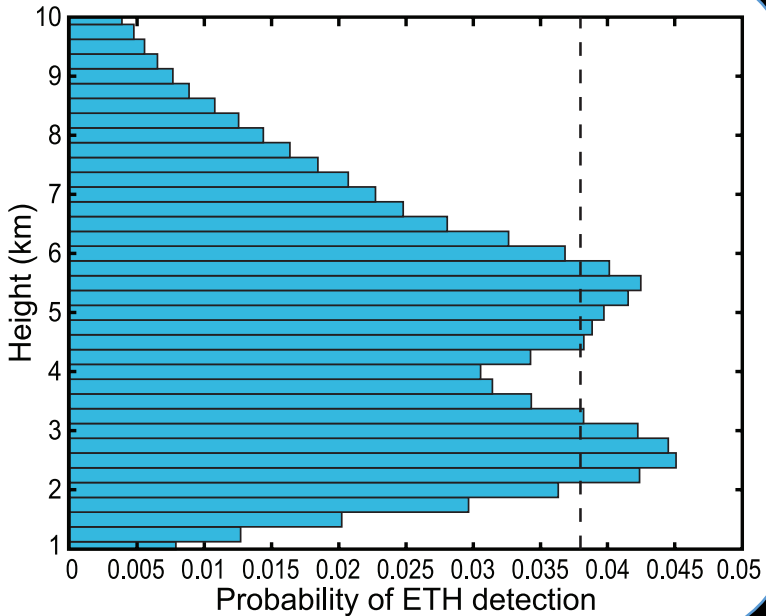


FIG. 5. As in Fig. 4b, but for divergence (shading,  $10^{-6} \text{ s}^{-1}$ ) and vertical velocity (contours,  $10^{-3} \text{ hPa s}^{-1}$ ; solid lines indicate positive values) anomalies calculated using ERA-Interim data.

Zuluaga and Houze  
(2013)





TRMM 20dBZ echo tops: 9N–9S; 60–100E

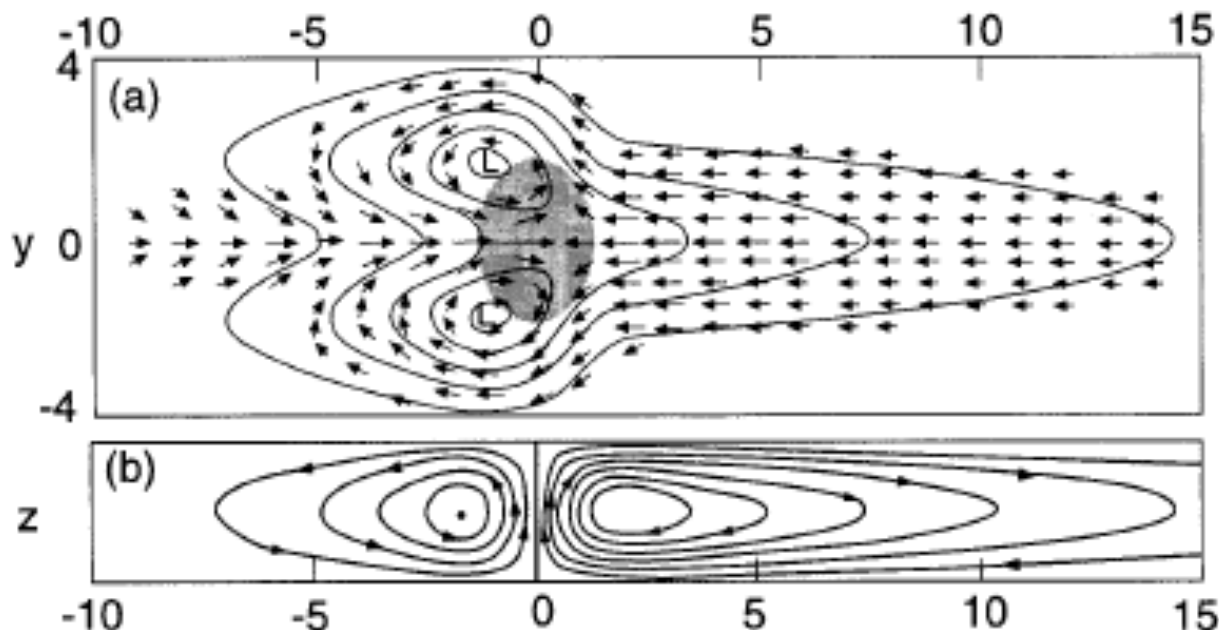


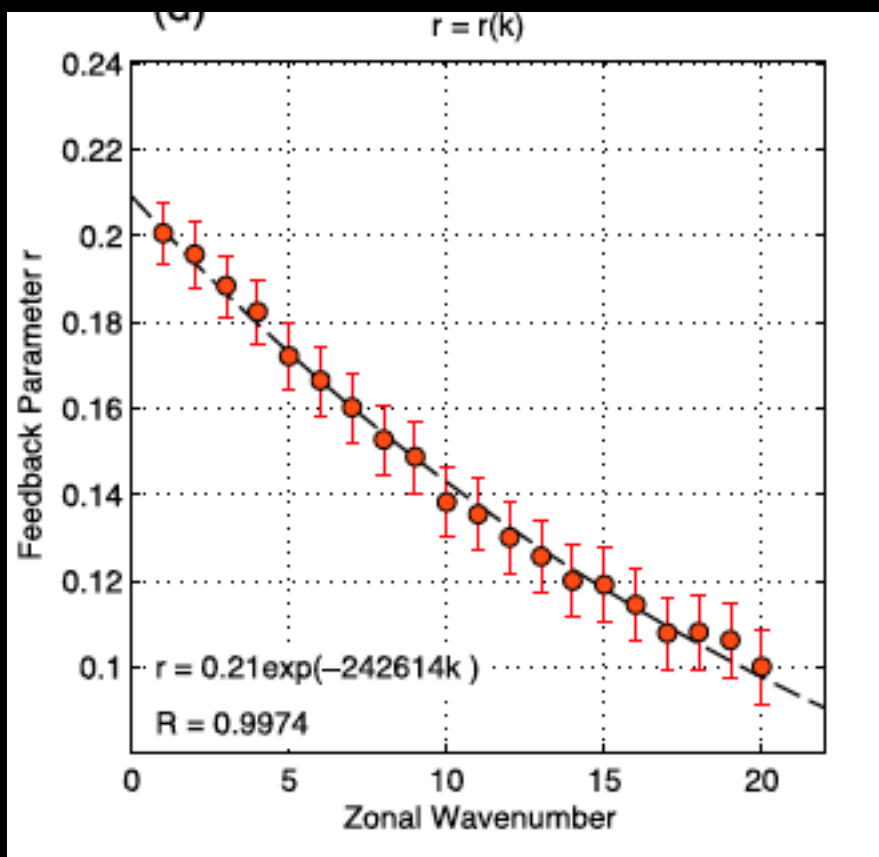
FIG. 1. Zonally asymmetric circulation produced by a deep heating anomaly over the equator (stippled). (a) Plan view of surface motion. (b) Streamlines in a vertical cross section over the equator. (From Gill 1980 as shown by Salby 1996.)

$$A_K = \frac{\sqrt{2}}{2} \delta q_u \hat{V}(1+r) \quad \text{and}$$

$$A_R = \sqrt{2}(\delta q_u + 2n\bar{q}_0 L^{-1})\hat{V}(1+r),$$

$$A_{KR} = A_K + A_R$$

$$\tilde{M}_{\text{tot}}^* = \tilde{M}_{\text{eff}}^* - \frac{2\sqrt{2}}{3}\hat{V}n\bar{q}_0(1+r).$$



$$c_p = \frac{\tilde{p} A_{KR}}{\tau_c k^2} \quad \text{and}$$

$$c_g = -\frac{\tilde{g} A_{KR}}{\tau_c k^2},$$

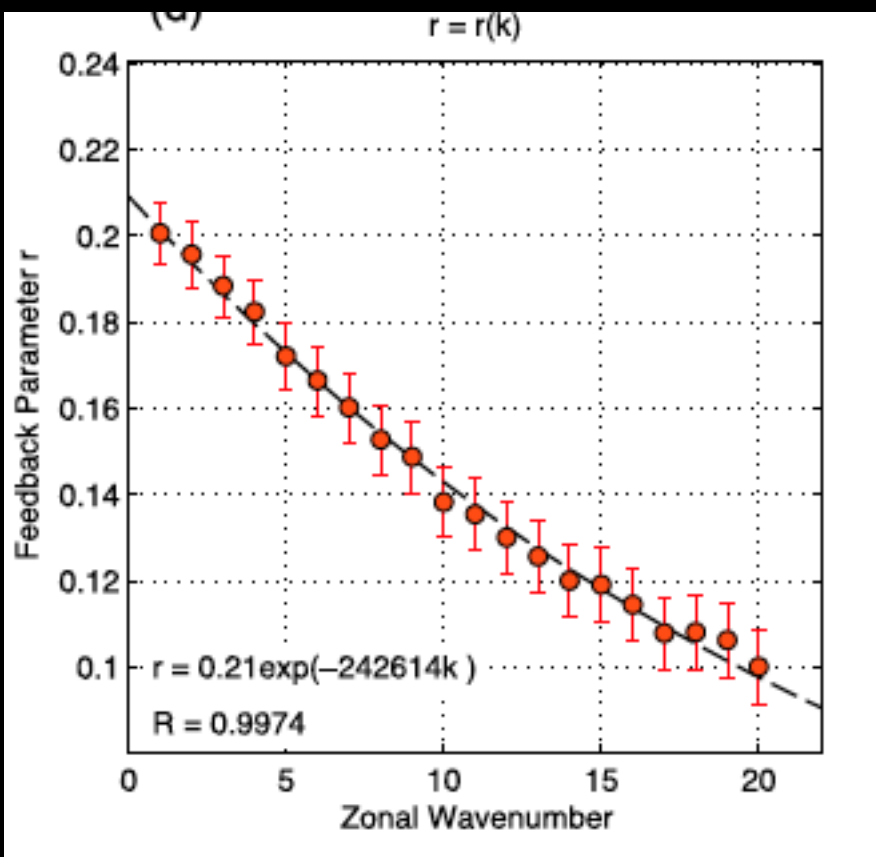
Adames and Kim (2016)

$$A_K = \frac{\sqrt{2}}{2} \delta q_u \hat{V}(1+r) \quad \text{and}$$

$$A_R = \sqrt{2}(\delta q_u + 2n\bar{q}_0 L^{-1})\hat{V}(1+r),$$

$$A_{KR} = A_K + A_R$$

$$\tilde{M}_{\text{tot}}^* = \tilde{M}_{\text{eff}}^* - \frac{2\sqrt{2}}{3}\hat{V}n\bar{q}_0(1+r),$$



$$c_p = \frac{\tilde{p}A_{KR}}{\tau_c k^2} \quad \text{and}$$

$$c_g = -\frac{\tilde{g}A_{KR}}{\tau_c k^2},$$

Adames and Kim (2016)

~50–70% of rainfall

~15–20% of rainfall

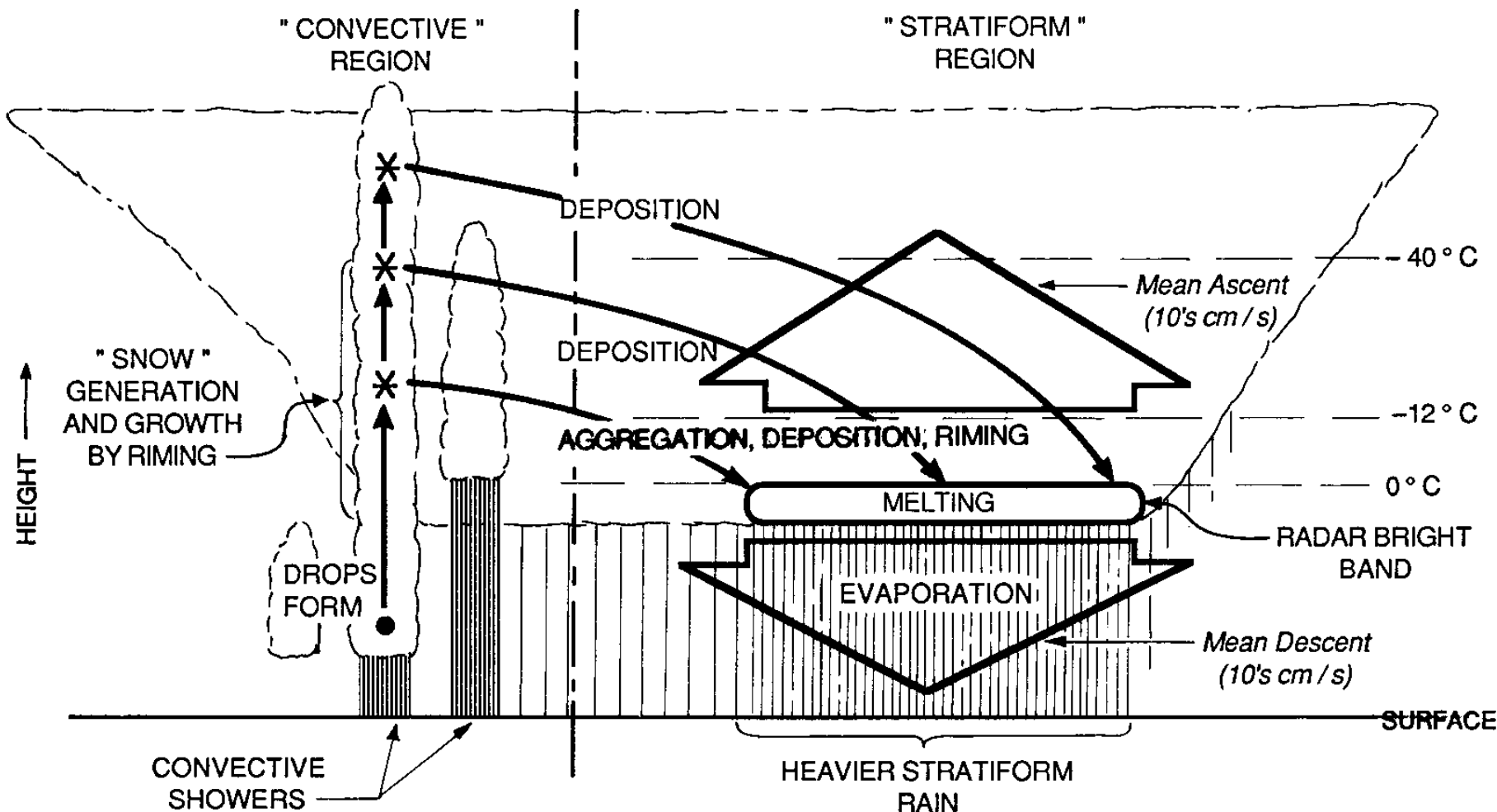


Figure 2. Schematic diagram of the precipitation mechanisms in a tropical cloud system. Solid arrows indicate particle trajectories (adapted from Houze 1989).

